ESR evidence for two coexisting liquid phases in deeply supercooled bulk water

D. Banerjee *, S. N. Bhat *, S. V. Bhat *, and D. Leporini † ‡

*Department of Physics, Indian Institute of Science, Bangalore 560 012, India,†Dipartimento di Fisica "Enrico Fermi", Università di Pisa, Largo B. Pontecorvo 3, I-56127 Pisa, Italy, and ‡SOFT-INFM-CNR, Largo B. Pontecorvo 3, I-56127 Pisa, Italy

Using Electron Spin Resonance spectroscopy (ESR), we measure the rotational mobility of probe molecules highly diluted in deeply supercooled bulk water and negligibly constrained by the possible ice fraction. The mobility increases above the putative glass transition temperature of water, $T_g = 136K$, and smoothly connects to the thermodynamically stable region by traversing the so called 'no man's land' (the range $150 - 235$ K), where it is believed that the homogeneous nucleation of ice suppresses the liquid water. Two coexisting fractions of the probe molecules are evidenced. The two fractions exhibit different mobility and fragility, the slower one is thermally activated (low fragility) and is larger at low temperatures below a fragile-to-strong dynamic crossover at $\sim 225K$. The reorientation of the probe molecules decouples from the viscosity below $\sim 225K$. The translational diffusion of water exhibits a corresponding decoupling at the same temperature [Chen S-H, et al. (2006) The violation of the Stokes-Einstein relation in supercooled water. Proc. Natl. Acad. Sci. U.S.A. 103: 12974-12978]. The present findings are consistent with key issues concerning both the statics and the dynamics of supercooled water, namely the large structural fluctuations [Poole PH , Sciortino F , Essmann U, Stanley HE (1992) Phase behaviour of metastable water. Nature 360: 324-328] and the fragile-to-strong dynamic crossover at $\sim 228K$ [Ito K, Moynihan CT, Angell CA (1999) Thermodynamic determination of fragility in liquids and a fragile-to-strong liquid transition in water. Nature 398:492-494].

supercooled water | Electron Spin Resonance spectroscopy | dynamic heterogeneity | decoupling of transport properties | dynamic cross-over in water

Abbreviations: DH , dynamical heterogeneity; DSE , Debye-Stokes-Einstein law; ESR, Electron Spin Resonance spectroscopy; FSC, fragile-to-strong dynamic crossover; HDL , high-density liquid; LDL, low-density liquid; SE , Stokes-Einstein law; NML, no man's land; OTP, o-terphenyl; TEMPOL, 4-hydroxy-2,2 ,6,6-tetramethylpiperidine-1-oxyl

The physical properties of water are far from being completely understood. Several thermodynamic and dynamic anomalies are known or anticipated in the metastable supercooled regime which influence the equilibrium states and have deep impact in biology, astrophysics, glaciology and atmospheric science [1, 2, 3]. At ambient pressure the supercooled regime ranges between the commonly accepted value of the glass transition temperature $T_g = 136K$ and the freezing temperature $T_m = 273.15K$. Above T_g amorphous water transforms into a highly viscous fluid [4, 5]. Crystallization into metastable cubic ice (I_c) at $T_X \sim 150K$ with further transformation to the usual hexagonal form of ice I_h is reported [1, 6]. On the other hand, bulk water at atmospheric pressure can be supercooled below its melting temperature down to the homogeneous nucleation temperature $T_H \sim 235K$, below which it usually crystallizes to I_h. Thus, the region between T_X and T_H is often regarded as a region where liquid water cannot be observed ("no man's land" , NML [1]). Nonetheless, the coexistence of crystals and deeply supercooled liquids was suspected almost one century ago for bulk systems [7]. More recently, evidence that water and cubic ice coexist in thin films in the temperature range $140 - 210K$ was reported [8, 9, 10, 11]. The existence of liquid water has been also shown experimentally in veins (or so-called triple junctions) of polycrystalline ice [12] which serve as interfacial reservoirs for impurities [13, 14, 15]. The size of such reservoirs is thermodynamically defined by surface forces, and also by the curvature of the surface (i.e., the Kelvin effect in veins) [11, 16]. In pure ice, the reservoir size increases when approaching the melting point [17].

This background motivated us to investigate the coexistence of ice and supercooled water in large volumes in an attempt to characterize the dynamical properties of the liquid, particularly in NML. Of major interest is the comparison with the results concerning the liquid behavior evidenced in small volumes, like nanopores [18, 19, 20] and nanometric films [4, 10], where homogeneous nucleation is bypassed.

NML is of paramount interest for a definitive picture of the supercooled water. Different scenarios predict their characteristic temperatures in NML, i.e. the singular temperature $T_s \sim 228K$ where most response functions appear to diverge [3], the fragile-to-strong dynamic crossover (FSC) temperature at $T_{FSC} \sim 228K$ [6, 21, 22], the strongly suspected second critical point at $T_c \sim 220K$, $P_c \sim 10^8 Pa$ [23] and the kinetic glass transition temperature $T_{MCT} \sim 221K$ [24, 25], The existence of characteristic temperatures highlights that viscous water close to T_g and normal water under equilibrium conditions are distinct, particularly due to the different *static* structural heterogeneities of the low- (LDL) and the high-density (HDL) states of water, the corresponding liquids of LDA and HDA amorphs [1, 2, 3, 19, 20, 26]. Viscous water is more structured and LDL-rich, whereas normal water is disordered and HDL-rich. This viewpoint is challenged by experimental results suggesting that supercooled water above T_g is an ultraviscous fragile liquid smoothly connected to the equilibrium states above the melting temperature T_m [4]. As further example of the unusual properties of water in NML, the breakdown of the Stokes-Einstein law (SE), stating the constance of the quantity $\mathcal{R}_{SE} \equiv D\eta/T$ (T, D, η being the temperature, the translational diffusion coefficient and the viscosity, respectively) , has been evidenced at $\sim 225K$ by confining water in nanopores [18] and simulations [26, 27, 28]. That decoupling has been attributed to the occurrence of *dynamical* heterogeneity (DH), i.e. a spatial distribution of mobility, in structural glass formers and put into correspondence with the *static* structural heterogeneities of water [26].

Orientation and reorientation of water molecules deserve consideration. There is competition between orientational entropy and bond energy in water and the anomalies of the latter are thought to be closely related to the orientational order [26, 29]. The rotation of individual water molecules, mainly occurring by large jumps ($\theta \simeq 60°$) [30], changes constantly the connectivity of the H-bond network. Recent simulations [26, 27, 28] suggested that the SE breakdown in water

Reserved for Publication Footnotes

must also be accompanied by the breakdown of the Debye-Stokes-Einstein law (DSE), accounting for the coupling between the viscosity and the rotational diffusion, as observed in experiments [31] and simulations [32] on molecular glassformers.

Outine of ESR spectroscopy

Electron Spin Resonance (ESR) spectroscopy detects the dynamics of the magnetization M of an ensemble of electrons in the presence of a static magnetic field B_0 and under driving by (ideally) a rotating magnetic field $B_1(t) \perp B_0$ with angular frequency ω (typically $\omega/2\pi \sim 9GHz$) [33]. The electron has magnetic dipole moment m which stems from its intrinsic angular moment (spin) $\hbar S$ with $\hbar = h/2\pi$, h being the Planck constant. For a free electron $m = -g_e\beta_e S$ where $g_e = 2.0023$ and β_e are the electron Lande' g-factor and the Bohr magneton, respectively. If $B_1(t) = 0$ and the spins are isolated, M, if misaligned with respect to B_0, performs a precession around B_0 with angular Larmor frequency $\omega_0 = \gamma B_0$ where $\gamma = g_e\beta_e/\hbar$ is the magnetogyric ratio (Fig.1a). The ESR spectroscopy usually investigates condensed-matter systems where the electrons exchange energy with the surroundings. When the rotating field $B_1(t)$ is acted on the magnetization M, the latter undergoes a precession around B_0 with angular frequency ω in the stationary state (fig.1b). For $\omega \simeq \omega_0$ a resonance is observed corresponding to a marked power absorption by the spin system.

Spin probes. Liquids are usually diamagnetic and then provide no ESR signal. The issue is circumvented by dissolving paramagnetic guest molecules (spin probes), usually nitroxide free radicals with one unpaired electron, at an extremely low concentration to make their influence on the host and their mutual interactions vanishingly small [33]. The unpaired electron is localized in a highly directional, i.e. anisotropic, molecular bond (see Fig.2). On this basis, a quantum-mechanical analysis shows that the Larmor frequency of the dipole moment of the spin probe depends on the orientation of the latter with respect to B_0 (see Supporting Information (SI)).

Rigid-limit and motional narrowing of the lineshape. We now illustrate how the ESR lineshape conveys information on the rotational dynamics of the spin probe [33, 34, 35]. Additional details are found in SI. We first consider an ensemble of immobile spin probes, e.g. like in a frozen host, with *different* fixed orientations. The *different* resonances of their magnetic dipole moments are detected by sweeping the ω frequency of $B_1(t)$ and their superposition gives rise to a broad absorption with width $\Delta\omega_0$, usually referred to as rigid-limit or powder lineshape (fig.1c). If the spin probe undergoes a rotational motion, the Larmor frequency of the associated dipole changes randomly in time. Fig.1d pictures the case of a reorientation occurring by sudden jumps separated by random waiting times with average value τ (τ denotes the rotational correlation time, i.e. the area below the normalized correlation function of the spherical harmonic $Y_{2,0}$ [34], see SI). The fluctuation gives rise to frequency averaging. In fact, let us consider two Larmor frequencies differing by $\delta\omega_0$. If the accumulated phase difference in a time τ, $\delta\omega_0\tau$, is less than one, the two frequencies cannot be distinguished and are replaced by their average. This process distorts the rigid-limit lineshape to an extent which is controlled by the product $\tau\Delta\omega_0$. Illustrative cases are shown in Fig.1d. If $\tau\Delta\omega_0 \gg 1$ the rigid-limit lineshape is rounded off on the frequency scale $1/\tau$. If $\tau\Delta\omega_0 \sim 1$, the average process manifests as a coalescence of the lineshape ("motional narrowing") which becomes extreme for $\tau\Delta\omega_0 \ll 1$. In the latter case the width of a single line is roughly given by $\Delta\omega_0^2\tau$ [34].

Accessible range of the rotational dynamics. The longest detectable τ value of a nitroxide spin probe by ESR, τ_{max}, is set by the changes of the Larmor frequency, occurring each $T_2^\star \sim 0.1\mu s$ on average, due

to the magnetic field produced by the rotating methyl groups close to the unpaired electron [33]. If $\tau \gg \tau_{max} \equiv T_2^\star$ the spin probe does not rotate within $T_2^\star$ appreciably, the lineshape is independent of the reorientation rate $1/\tau$ and virtually coincident with the rigid-limit lineshape. On the other hand, in the extreme narrowing regime the line coalescence cannot lead to linewidth less than $\sim 1/T_2^\star$ in that $T_2^\star$ is the upper limit of the lifetime of the coherent oscillation of the magnetization [33]. Then, the shortest detectable τ value, τ_{min}, is found when the linewidth $\Delta\omega^2\tau_{min} \sim 1/T_2^\star$. For nitroxide spin probes $\tau_{min} \sim 10ps$.

Results and Discussion

Samples were prepared in a capillary (dia $\sim 100\mu m$) by doping a small amount of triple distilled water with about 0.1% by weight of the polar spin probe TEMPOL, see Fig.2. The ESR signal of TEMPOL is recorded during the slow reheating of the quenched sample. Details are given in Methods Section.

Influence of the crystallization. In occasional runs the crystallization occurring during the thermal cycle affects the ESR signal of the spin probes. The resulting artifacts are well known in aqueous solutions [13, 14, 36] and due to the possible strong confinement of the radicals in interstices between the ice grains with subsequent strong reduction of their mutual distance (see Methods). However, in most runs the signal is flawless. Henceforth, we focus on these cases where strong arguments lead to the conclusion that the ice loosely confines TEMPOL in liquid pockets.

Spin-probe mobility above 130 K. Fig.2 presents the temperature-dependence of the ESR signal of the spin probe. As usual, the lineshape, due to phase-detection, is displayed in derivative mode by sweeping the static magnetic field B_0 with constant microwave frequency ω. * The lineshapes in Fig.2 are strikingly similar to the usual ones of spin probes dissolved in viscous liquids [14, 31, 33, 36, 37, 38]. At low temperatures ($\leq 90K$) the ESR lineshape exhibits the rigid-limit pattern, namely the reorientation of TEMPOL is very slow (rotational correlation time $\tau \gtrsim \tau_{max} \sim 0.1\mu s$). Above $120K$ the ESR lineshape changes and its "motional narrowing" becomes apparent signaling the increased mobility of the spin probe. For $T \gtrsim 220K$ narrowing is extreme and the lineshape collapses to three lines. The three-lines pattern connects *smoothly* to the one detected in equilibrium condition at $300K$. Note that the observed *narrowing* of the lineshape is opposite to the crystallization-driven *broadening* discussed above.

The temperature dependence of the ESR lineshape shown in Fig. 2 excludes the possibility that the spin probes are trapped into the solid *crystalline* matrix developed during the initial quench-cooling or the subsequent slow re-heating (when the ESR data are collected). In fact, if trapping occurs during the quench, the rigid-limit ESR lineshape at $90K$ should be observed on heating up to T_m, where a sudden collapse to a three-line pattern much similar to the one observed at $300K$ should occur due to the large increase in mobility. Instead, one notes the *continuous* narrowing of the lineshape, i.e. the progressively increasing mobility of TEMPOL, across the supercooled region from, say, $120K$ up to $300K$. Moreover, the motionally-narrowed lineshape at $220K$, pointing to fast reorientation, is almost identical to the one at $300K$ indicating that TEMPOL has similar mobility at that temperatures. Since fast reorientation is also seen between $220K$ and T_m (see below), the trapping of the spin probes into the ice fraction can be safely ruled out. Instead, it has to be concluded that, when ice freezes, TEMPOL, as most impurities [13, 14, 15], is expelled from the ice and accumulate in liquid pockets [7, 8, 9, 10, 11, 12, 16, 17]. The volume

---

* This results in a different pattern with respect to the one in Fig.1d where for clarity's sake ω is swept with B_0 constant, no derivative operation is perfomed, and the coupling of the unpaired electron with the nuclear magnetic dipoles has been neglected (see SI for details).

fraction of the liquid water ϕ_w is estimated to be $\phi_w \gtrsim 0.04 - 0.07$ (see Methods).

Dynamical heterogeneities. In-depth numerical analysis of the ESR lineshape was first carried out by modeling the jump reorientation of TEMPOL in terms of the jump angle θ and the rotational correlation time τ (see Methods). When fitted to the experiment, the model, relying on a *homogeneous* mobility scenario, worked nicely except in the temperature region $140 - 180K$ and typical results are shown in Fig.2. In the temperature region $140 - 180$ K dynamical heterogeneity (DH) is apparent. In fact, entering the DH regime on heating, a second component, to be ascribed to a TEMPOL fraction with *greater* rotational mobility, appears (Fig.3). In the DH regime the lineshape was evaluated as a weighted sum of two components, i.e. the "fast" (F) component with weight w_f and the "slow" (S) component with weight $w_s = 1 - w_f$. On increasing the temperature, w_f increases and above $180K$, still well inside NML, $w_f \simeq 1$ (see b inset of Fig.4). The missing evidence of heterogeneous dynamics above 180 K is due to the limited ability of the ESR spectroscopy to discriminate between different TEMPOL rotational mobilities if the correlation times are too short ($\tau \lesssim 1ns$) and cannot be taken as evidence of no actual DH.

Temperature dependence of the spin-probe reorientation. Fig.4 presents the temperature dependence of the model parameters describing the reorientation of the two TEMPOL fractions. It is seen that at the lowest temperatures the dominant S fraction of TEMPOL undergoes small-size diffusive rotational jumps with nearly constant τ_s correlation times. Crossing over $127K$, τ_s starts to drop and the jump size to increase which is consistent with a more mobile and open structure of the surroundings of TEMPOL consequent to the glass transition. At $140K$ the F component becomes apparent in the ESR lineshape and its weight increases with the temperature. The presence of the F fraction leads to no anomaly in the rotational dynamics of TEMPOL molecules belonging to the S fraction. In particular, θ_s levels off to $\simeq 60°$ (see Fig.4a) in agreement with simulations on water [30]. The DH region ends at about $180K$ above which only the F component is seen. The correlation time τ_f decreases with the temperature and shows an inflection point at about $225K$. At higher temperatures τ_f connects *smoothly* to the equilibrium value at $300K$.

We note that the temperature dependence of the TEMPOL correlation times in Fig.4 shows a crossover at $225K$ from a high-temperature "fragile" behaviour (non-Arrhenius) to a lower-temperature "strong" one (Arrhenius) which strongly resembles the FSC crossover which has been hypothesized for water at $T_{FSC} \sim 228K$ [6] with recent support from simulation [21] and experiments in confined environments [22]. The observation of fragile behaviour in weakly supercooled water is fully consistent with the views that the water glass transition is kinetic in nature [24, 25],

Breakdown of the Debye-Stokes-Einstein law. Both the FSC and DH in supercooled water drive the breakdown of the SE and DSE relations [18, 26, 27, 28]. The DSE breakdown was already observed by ESR in supercooled liquids [31]. We evaluated the DSE ratio $\mathcal{R}_{DSE} \equiv \eta/(\tau_f T)$ (to be constant according to the DSE law). To evaluate the water viscosity below $T_H \sim 235K$, we resorted to, after proper consideration (see Methods), a thermodynamic construction [39] based on the entropy-based Adam-Gibbs equation [40, 41]. Owing to the several thermodynamic constraints on the entropy of water, the construction provides tight bounds on $\eta(T)$ below T_H provided that a maximum in the specific heat occurs at about $225K$ [39]. The latter has been recently observed [42]. Fig.5 shows the results about $\mathcal{R}_{DSE}$ which are compared to the corresponding SE ratio $\mathcal{R}_{SE}$ for nanoconfined water [18]. At high temperatures both SE and DSE are weakly violated. In fact, the ratio $\mathcal{R}_{DSE}$ increases by about 5.1 times from $280K$ down to $240K$ (the water viscosity increases by about 16 times [39]), whereas $\mathcal{R}_{SE}$ increases by about 4.4 times for nanocon-

fined water [18]. By decreasing the temperature below $\sim 225K$ one observes that both $\mathcal{R}_{DSE}$ and $\mathcal{R}_{SE}$ increase much more than at high temperature, i.e. the violations of both SE and DSE are much more apparent. So, we note that DSE, as SE (see also fig.3 of ref.[18]), undergoes a two-stage decoupling, i.e. a weak violation above $\sim 225K$ followed by a stronger decoupling at lower temperatures. The larger increase of $\mathcal{R}_{DSE}$ with respect to $\mathcal{R}_{SE}$ at lower temperatures is in agreement with simulations of water [27, 28] and molecular liquids (see [32] and ref.22 of that paper).

Spin-probe sensing of the water static heterogeneities. The correspondence between DH, the breakdown of SE and DSE and the presence of *static* heterogeneities in supercooled water, characterized by large fluctuations spanning a range of structures from HDL-like to LDL-like, has been explored with particular attention to the local orientational order [26, 27, 28]. It is interesting to put the evidence concerning the heterogeneous dynamics of TEMPOL within this context. In the low-temperature region of the supercooled regime, the LDL fraction, characterized by better organization of the local tetrahedrally coordinated hydrogen-bonded network, is higher than the HDL fraction where the network is not fully developed [19, 20]. One expects that LDL exhibits slower rearrangements and lower fragility (i.e. more Arrhenius-like temperature dependence) than HDL. The HDL fraction is larger at higher temperatures and connects smoothly to the equilibrium states above T_m [19, 20]. This scenario suggests that TEMPOL senses the distribution of static structures of supercooled water. In particular, the S fraction senses LDL and the F fraction senses HDL. In fact, i) the S fraction of TEMPOL reorientates with Arrhenius behaviour, whereas the F fraction is more fragile, i.e. τ_f exhibits a non-Arrhenius temperature dependence (see Fig.4); ii) the weight of the F fraction increases with the temperature and connects smoothly to the reorientation regime of TEMPOL above T_m.

ESR evidences LDL and HDL states of water in an indirect way via their influence on the spin-probe reorientation. This raises the question of their direct identification in the supercooled water-ice mixture. To do that, one needs a technique with good discrimination between the three distinct coexisting contributions, i.e. ice, LDL and HDL. From this respect, promising opportunities are offered by: i) the measurement of the vibrational spectra (HOH bending and OH-stretching modes) via Fourier transform infrared spectroscopy (see Fig.1b of ref. [19]) and ii) the measurement of the proton chemical shift δ_{NMR} by NMR providing a picture of the intermolecular geometry (compare the data of Fig 1a of ref. [42] with $\delta_{NMR} = 7.4ppm$ for a single crystal of hexagonal ice [43]).

In conclusion, ESR investigations of the rotational mobility of probe molecules dissolved in deeply supercooled bulk water provide evidence for two coexisting liquid phases between ~ 130K and the thermodynamically stable region, including the 'no man's land' (the range $150 - 235$ K). Two distinct fractions of the probe molecules with different mobility and fragility are observed. It is argued that they sense the low- and the high-density states of supercooled water. The reorientation of the probe molecules exhibits fragile, i.e. non-Arrhenius, character at high temperature with a crossover to a strong behaviour below ~ 225K. An analogous crossover has been hypothesized for water at $T_{FSC} \sim 228$K [6]. The temperature dependence of the correlation time of the slow component shows a change in slope at ~ 127 K, close to the putative glass transition temperature of water at ~ 136 K. The reorientation of the probe molecules decouples from the viscosity below ~ 225 K (DSE breakdown), paralleling the behaviour of the translational diffusion of water [18].

Materials and Methods

Samples were prepared in a capillary (dia $\sim 100\mu m$) by doping a small amount of triple distilled water with about 0.1% by weight of the polar radical TEMPOL (spin probe). TEMPOL accommodates well in water due to hydrogen-bonds and the moderate size ($r_{TEMPOL} \sim 0.34\,nm$ to be compared to

$r_{H2O} \sim 0.14\,nm$). The amorphous water samples were prepared by direct exposition to liquid helium $(4.2K)$ *in situ* in the ESR low temperature cryostat. The liquid helium transfer tube was modified such that a burst of liquid helium hits the capillary cooling it to $4.2K$ almost instantaneously leading to the formation of vitrified water.

The ESR signal of TEMPOL are recorded by using a X-band Bruker ER 200 CW EPR spectrometer. Data are collected on heating the quenched samples. At a selected temperature no aging, i.e. no sample evolution, was ever detected.

The ESR lineshape provides information on the conditions of the sample during the experiment, particularly the degree of confinement of the spin probe between the ice grains and the amount of the interstitial liquid water above $130K$. In fact, the spin probes, as most impurities [13, 14, 15], are expelled from the ice grains and accumulate in the interstitial liquid fraction. This process reduces the mutual distances between the radicals and, if the confinement is strong, leads to the huge increase of the ESR linewidth [13, 14, 36]. In fact, at short distances the magnetic field $\boldsymbol{B}^{(sp)}$ created by one spin probe is not negligible ($|\boldsymbol{B}^{(sp)}| \sim 150$ Gauss at $0.5\,nm$ [33]). Then, each spin probe sees an effective total magnetic field due to the surrounding ones $\boldsymbol{B}_0^{\star} \sim \boldsymbol{B}_0 + \Sigma_j \boldsymbol{B}_j^{(sp)}$. Due to the randomness of both the direction and the modulus of $\boldsymbol{B}_i^{(sp)}$, $|\boldsymbol{B}_0^{\star}|$ exhibits a distribution centered at B_0 and width about $|\boldsymbol{B}_{sp}|$ resulting in a very wide distribution of the Larmor frequencies $\omega_0 \propto |\boldsymbol{B}_0^{\star}|$, i.e. an apparent line broadening exceedingly larger than the one observed under diluted conditions. In our experiments the line broadening due to the crystallization was observed only occasionally during the several experimental runs. This points to the conclusion that the crystallization does not yield a marked increase of the spin probe concentration in the liquid fraction of the water-ice mixture. The minimum liquid fraction ϕ_w of the sample which is needed not to observe crystallization effects on the ESR lineshape may be estimated. Let us assume that, due to the increased spin probe concentration, the magnetic field $\boldsymbol{B}^{(sp)}$ acted by one spin probe on the close ones is large enough to exceed any other broadening effect. At $220K$ the narrowest line of the observed triplet has width of about $1-2$ Gauss (see Fig.2). If the spin probes, with magnetic dipole equal to about the Bohr magneton μ_B, have mutual average distance d, $B^{(sp)} \propto \mu_B d^{-3}$ and $B^{(sp)} \sim 1-2$ Gauss if $d \sim 2.1 - 2.6\,nm$. If no ice is present, TEMPOL molecules are homogeneously dispersed in water with, given the adopted concentration, average distance $d' \simeq 6.4\,nm$. Then, $\phi_w \geq (d/d')^3 \sim 0.04 - 0.07$.

The lineshape is evaluated by a stochastic memory-function approach (see SI and ref.[35]). The reorientation of TEMPOL, due to its globular shape, is modeled by instantaneous random jumps with fixed size θ after a mean residence time τ_0 [38]. Under this hypothesis, the rotational correlation time τ (the area below the normalized correlation function of the spherical harmonic $Y_{2,0}$ [34]) is given by $\tau = \tau_0/[1 - \sin(5\theta/2)/5\sin(\theta/2)]^{-1}$. The temperature-independent magnetic parameters of TEMPOL were determined by the rigid-limit lineshape recorded at low temperature according to a procedure detailed elsewhere [44] and outlined in SI. The number of adjustable parameters of the theoretical lineshape changes over the temperature range under investigation. In general, the ESR lineshape is fitted by using two components, corresponding to the fast (F) and slow (S) fractions of TEMPOL, with weights w_f and $w_s = 1 - w_f$, respectively. The S component depends on two adjustable parameters, i.e. τ_s and θ_s, whereas, due to rapid motion, the F component depends on τ_f only. Therefore, to fit the ESR lineshape in the temperature region $140 - 180K$ (DH regime) one needs four adjustable parameters $(\tau_s, \theta_s, \tau_f, w_f)$. These reduce to two (τ_s, θ_s) at lower temperatures where $w_s \simeq 1$ and one (τ_f) to higher temperatures where $w_f \simeq 1$. The theoretical lineshape was convoluted by a gaussian curve with width $1/T_2^{\star}$ to account for the magnetic field produced by the rotating methyl groups close to the unpaired electron. $T_2^{\star}$ increases with the temperature from ~ 30 ns up to ~ 40 ns in the temperature range $90K - 300K$.

To get confidence on the thermodynamic extrapolation of the viscosity below $T_H \sim 235K$ [39] we compared the DSE violation of TEMPOL in water with the one of the spin probe TEMPO (virtually identical to TEMPOL) in the prototypical fragile glassformer o-terphenyl (OTP) where η is known [31]. At the temperature where the DSE violation takes place ($225K$ for TEMPOL in water and $290K$ for TEMPO in OTP) $\mathcal{R}_{DSE}(TEMPO)/\mathcal{R}_{DSE}(TEMPOL) \sim 1.33$. If one considers temperatures where water and OTP have viscosities 10^{11} times larger than the ones where the DSE breakdown is observed (about $170K$ for water and $240K$ for OTP), one has $\mathcal{R}_{DSE}(TEMPO)/\mathcal{R}_{DSE}(TEMPOL) \sim 1.08$. This comparison shows that the magnitude of the DSE breakdown in water and OTP is quite similar and reassured us on the robustness of extrapolation.

1. Mishima O, Stanley HE (1998) The relation between liquid, supercooled and glassy water. *Nature* 396: 329-335.
2. Debenedetti PG (2003) Supercooled and glassy water. *J. Phys.:Condens.Matter* 15: R1669-R1726 .
3. Angell CA (2008) Insights into Phases of Liquid Water from Study of Its Unusual Glass-Forming Properties. *Science* 319: 582-587 .
4. Smith RS , Kay BD (1999) The existence of supercooled liquid water at $150K$. *Nature* 398: 788-791 .
5. Johari GP (1998) Liquid State of Low-Density Pressure-Amorphized Ice above Its Tg. *J. Phys. Chem. B* 102: 4711-4714 .
6. Ito K, Moynihan CT, Angell CA (1999) Thermodynamic determination of fragility in liquids and a fragile-to-strong liquid transition in water. *Nature* 398: 492-495 .
7. Rosenhain W, Ewen D (1913) The intercrystalline cohesion of metals. *J.Inst.Metals* 10: 119-148 .
8. Dowell LG, Rinfret AP (1960) Low-temperature forms of ice as studied by X-ray diffraction. *Nature* 188: 1144-1148 .
9. Jenniskens P, Banham SF, Blake DF , McCoustra MRS (1997) Liquid water in the domain of cubic crystalline ice I_C. *J. Chem. Phys.* 107: 1232-1241 .
10. Souda R (2007) Two Liquid Phases of Water in the Deeply Supercooled Region and Their Roles in Crystallization and Formation of LiCl Solution. *J. Phys. Chem. B* 111: 5628-5634 .
11. Johari GP (1998) Thermodynamics of water-cubic ice and other liquid-solid coexistence in nanometer-size particles. *J. Chem. Phys.* 109: 1070-1073 .
12. Mader HJ (1992) The thermal behaviour of the water-vein system in polycrystalline ice. *J. Glaciology* 38: 359-374.
13. Ross RT (1965) Dipolar broadening of EPR spectra due to solute segregation in frozen aqueous solution. *J.Chem.Phys.* 42:3919-3922.
14. Leigh JS Jr., Reed GH (1971) Electron paramagnetic resonance studies in frozen aqueous solutions. Elimination of freezing artifacts. *J. Phys. Chem.* 75: 1202-1204.
15. Mulvaney R, Wolff EW, Oates K (1988) Sulphuric acid at grain boundaries in Antarctic ice. *Nature* 331: 247-249.
16. Nye JF (1991) Thermal behaviour of glacier and laboratory ice. *J. Glaciology* 37: 401-413.
17. Wettlaufer JS, Grae Worster M (2006) Premelting Dynamics. *Annu. Rev. Fluid. Mech.* 38: 427-452.
18. Chen S-H, *et al.* (2006) The violation of the Stokes- Einstein relation in supercooled water. *Proc. Natl. Acad. Sci. U.S.A.* 103: 12974-12978 .
19. Mallamace F, *et al.* (2007) Evidence of the existence of the low-density liquid phase in supercooled, confined water. *Proc. Natl. Acad. Sci. U.S.A.* 104: 424Đ428.
20. Mallamace F, *et al.* (2007) The anomalous behavior of the density of water in the range $30K < T < 373K$. *Proc. Natl. Acad. Sci. U.S.A.* 104: 18387-18391.
21. Xu L, *et al.* (2005) Relation between the Widom line and the dynamic crossover in systems with a liquid-liquid phase transition. *Proc. Natl. Acad. Sci. USA* 102: 16558Đ16562 .
22. Liu L, Chen S-H, Faraone A, Yen C-W, Mou C-Y (2005) Pressure Dependence of Fragile-to-Strong Transition and a Possible Second Critical Point in Supercooled Confined Water. *Phys. Rev. Lett.* 95: 117802-4 .
23. Poole PH , Sciortino F , Essmann U, Stanley HE (1992) Phase behaviour of metastable water. *Nature* 360: 324-328 .
24. Sciortino F, Gallo P, Tartaglia P, Chen S-H (1996) Supercooled water and the kinetic glass transition. *Phys.Rev.E* 54: 6331-6343.
25. Torre R, Bartolini P, Righini R (2004) Structural relaxation in supercooled water by time-resolved spectroscopy. *Nature* 428: 296-299.
26. Kumar P , *et al.* (2007) Relation between the Widom line and the breakdown of the Stokes-Einstein relation in supercooled water. *Proc. Natl. Acad. Sci. U.S.A.* 104: 9575-9579.
27. Becker SR, Poole PH, Starr FW (2006) Fractional Stokes-Einstein and Debye-Stokes-Einstein Relations in a Network-Forming Liquid. *Phys. Rev. Lett.* 97: 055901-4 .
28. Mazza MG, Giovambattista N, Stanley HE, Starr F.W. (2007) Connection of translational and rotational dynamical heterogeneities with the breakdown of the Stokes-Einstein and Stokes-Einstein-Debye relations in water. *Phys. Rev. E* 76: 031203-12.
29. Errington JR, Debenedetti PG (2001) Relationship between structural order and the anomalies of liquid water. *Nature* 409: 318-321.
30. Laage D, Hynes JT (2006) A Molecular Jump Mechanism of Water Reorientation. *Science* 311: 832-835.
31. Andreozzi L, Di Schino A , Giordano M, Leporini D (1997) Evidence of a fractional Debye-Stokes-Einstein law in supercooled o-terphenyl. *Europhys. Lett.* 38: 669-674.
32. De Michele C, Leporini D (2001) Viscous flow and jump dynamics in molecular supercooled liquids. II. Rotations. *Phys. Rev. E* 63: 036702-10.

33. Weil JA, Bolton JR (2006) *Electron Paramagnetic Resonance: Elementary Theory and Practical Applications* (Wiley-Interscience, New York).

34. Nordio PL (1976) in *Spin labeling: theory and applications*, ed Berliner LJ (Academic Press, New York), pp 5-52.

35. Giordano M, Grigolini P, Leporini D, Marin P (1983) Fast computational approach to the evaluation of slow motion EPR spectra in terms of a generalized Langevin equation. *Phys.Rev.A* 28: 2474-2481.

36. Bhat SN, Sharma A , Bhat SV (2005) Vitrification and Glass Transition of Water; Insights from Spin Probe ESR. *Phys. Rev. Lett.* 95: 235702-4 .

37. Polnaszek CF, Bruno GV, Freed JH (1973) ESR lineshapes in the slow-motional region: Anisotropic liquids. *J.Chem.Phys.* 58:3185-3199.

38. Andreozzi L , Cianflone F , Donati C , Leporini D (1996) Jump reorientation of a molecular probe in the glass transition region of o-terphenyl. *J. Phys.: Condens. Matter* 8: 3795-3809.

39. Starr FW , Angell CA, Stanley HE (2003) Prediction of entropy and dynamic properties of water below the homogeneous nucleation temperature. *Physica A* 323: 51-66.

40. Angell CA (1997) Entropy and fragility in supercooling liquids. *J. Res. NIST* 102: 171-185.

41. Scala A, Starr FW, La Nave E, Sciortino F , Stanley HE (2000) Configurational entropy and diffusivity of supercooled water. *Nature* 406: 166 - 169.

42. Mallamace F, *et al.* (2008) NMR evidence of a sharp change in a measure of local order in deeply supercooled confined water. *Proc. Natl. Acad. Sci. U.S.A.* 105: 12725 12729.

43. Pfrommer BG, Mauri F, Louie SG (2000) NMR chemical shifts of ice and liquid water: the effects of condensation. *J. Am. Chem. Soc.* 122:123-129.

44. Andreozzi L, Giordano M, Leporini D (1993) Efficient characterization of the Orientational Ordering of ESR-active Probes in Supermolecular Fluids. *Appl.Magn.Reson.* 4: 279-295.
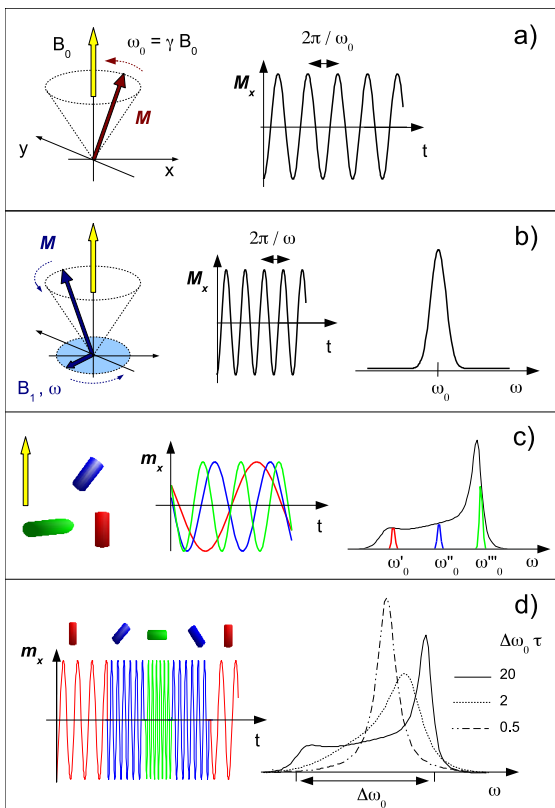
Fig. 1. Aspects of the ESR spectroscopy. a) free precession of the magnetization M of an ensemble of isolated electrons around the static magnetic field B_0 with Larmor angular frequency $\omega_0 = \gamma B_0$, γ being the magnetogyric ratio. The transverse magnetization oscillates at the same frequency. b) In condensed matter the electrons exchange energy with the surroundings. A rotating microwave field $B_1(t) \perp B_0$ with angular frequency ω forces the precession of the magnetization around B_0 with the same angular frequency. When $\omega \simeq \omega_0$ an absorption resonance occurs. c) The magnetic dipoles m of immobile spin probes in a frozen liquid have different ω_0 values due to their different orientations with respect to B_0, thus resulting in a broad line with width $\Delta\omega_0$ (black line), usually referred to as rigid-limit or powder lineshape. d) If the spin probe undergoes rotation (sketched as instantaneous clockwise jumps at random times), ω_0 fluctuates. When the rotational rate $1/\tau$ is larger than the width of the ω_0 distribution $\Delta\omega_0$, the different precession frequencies become indistinguishable and an average value is seen, i.e. the ESR lineshape coalesces (motional narrowing).
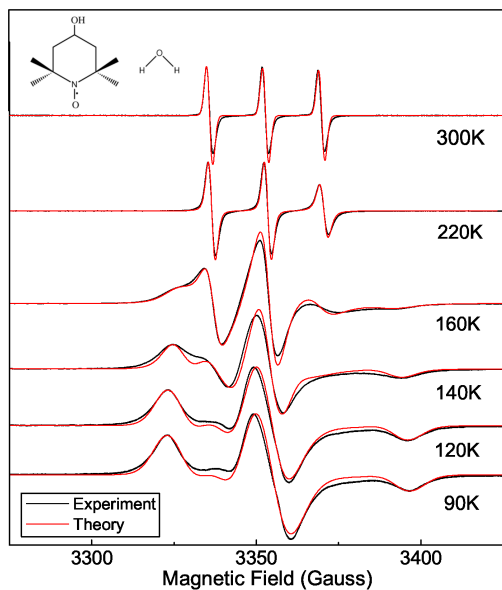
Fig. 2. Selected ESR lineshapes of the spin probe TEMPOL in quenched bulk water and subsequent re-heating at the indicated temperature. Note that: i) for technical convenience the static magnetic field B_0, and not the microwave frequency ω as in Fig.1, is swept; ii) the phase-sensitive detection displays the lineshape in derivative mode. The chemical structures of TEMPOL (molecular size $r_{TEMPOL} \sim 0.34\,nm$) and water ($r_{H2O} \sim 0.14\,nm$) molecules are sketched. The unpaired electron of TEMPOL (drawn as a dot) is localized in the NO bond. The theoretical predictions considering the reorientation of TEMPOL with $(140K, 160K)$ and without dynamical heterogeneity are also shown.
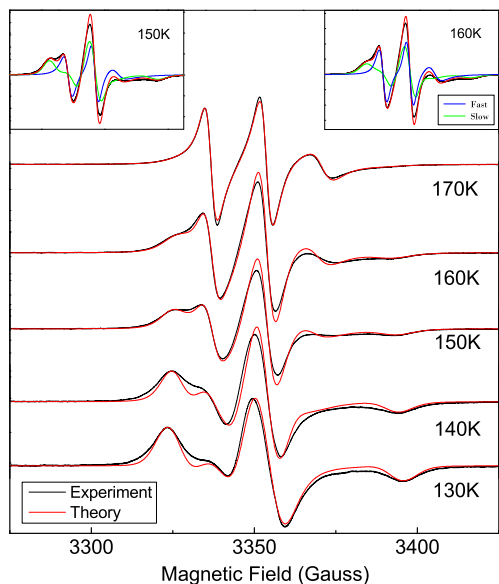

Fig. 3. ESR lineshapes of TEMPOL in DH regime. Note the growth of the narrow component (fast TEMPOL) which superimposes to the broader one (slow TEMPOL) with increasing temperature. The insets show the fast (blue) and slow (green) components of the overall lineshape (red) at two temperatures.
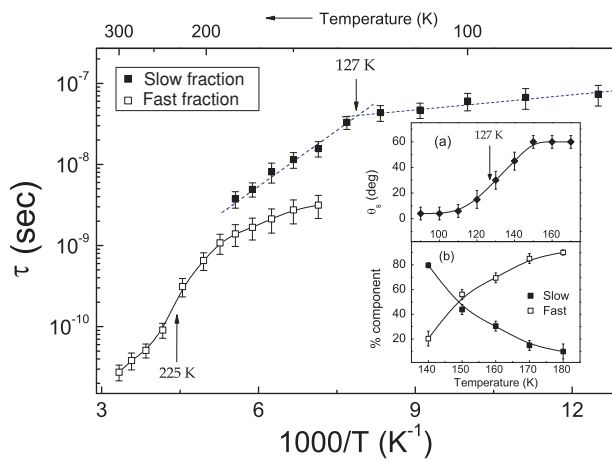
Fig. 4. Temperature dependence of the rotational parameters of the fast (F) and the slow (S) fractions of TEMPOL in deeply supercooled bulk water. Main panel: rotational correlation times τ_s and τ_f. Inset a: average jump angle of the S fraction. Inset b: weights of the F and S fractions. Note in the main panel : i) the knee at $\sim 127K$ close to $T_g = 136K$, ii) the DH regime $(140-180K)$ where the two coexisting TEMPOL fractions with different mobilities are evidenced, iii) the inflection close to $T_{FSC} \sim 228K$.
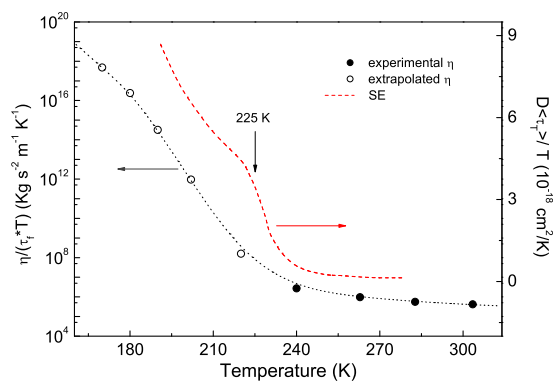

Fig. 5. Breakdown of the DSE law. Data are compared with the SE breakdown from ref.[18]. Filled dots refer to temperatures where experimental values of the viscosity are available. Empy dots are based on a thermodynamic extrapolation of the viscosity [39]. The line across the dots is a guide for the eyes.